# A myosin II-based nanomachine devised for the study of Ca$^{2+}$-dependent mechanisms of muscle regulation

**Irene Pertici [1], Giulio Bianchi [1], Lorenzo Bongini [1], Vincenzo Lombardi [1,* ] and Pasquale Bianco [1]**

[1] PhysioLab, University of Florence, 50019 Sesto Fiorentino (FI), Italy; irene.pertici@unifi.it (I.P.); giuli.bianchi@student.unisi.it (G.B.); lnzbng@gmail.com (L.B.); pasquale.bianco@unifi.it (P.B.)

\* Correspondence: vincenzo.lombardi@unifi.it; Tel.: +39-0554572388

**Abstract:**

The emergent properties of the array arrangement of the molecular motor myosin II in the sarcomere of the striated muscle, generation of steady force and shortening, can be studied *in vitro* with a synthetic nanomachine, made by an ensemble of eight HMM myosin fragments from rabbit psoas muscle carried on a piezoelectric nanopositioner and brought to interact with a properly oriented actin filament attached via gelsolin (a Ca$^{2+}$-regulated actin binding protein) to a bead trapped by a Dual Laser Optical Tweezers. The application of the original version of the nanomachine to investigation of the Ca$^{2+}$-dependent regulation mechanisms of the other sarcomeric (regulatory or cytoskeleton) proteins, adding them on at a time, was anyway prevented by the impossibility to preserve Ca$^{2+}$ as a free parameter. Here the nanomachine is implemented by assembling the bead-attached actin filament with the Ca$^{2+}$-insensitive gelsolin fragment TL40. The performance of the nanomachine is determined either in the absence or in the presence of 0.1 mM Ca$^{2+}$ (the concentration required for BTA preparation with gelsolin). The nanomachine exhibits a maximum power output of 5.4 aW, independently of [Ca$^{2+}$], opening the possibility for future studies of the Ca$^{2+}$-dependent function/dysfunction of regulatory and cytoskeletal proteins.

**Keywords:** myosin ensemble mechanics; myosin-based machines; synthetic nanomachines; dual laser optical tweezers

## 1. Introduction

In the sarcomere, the structural unit of the striated (cardiac and skeletal) muscle, two antiparallel arrays of the molecular motor myosin II extending from the thick filament pull the nearby thin, actin-containing, filaments from the opposite extremities of the sarcomere toward the centre (Fig. 1a). The individual myosin motors interact with actin only briefly, generating piconewton force and nanometer displacement of the actin filament through an ATP driven working stroke [1,2], and remain detached throughout most of their ATP hydrolysis cycle [3]. Production of steady force and shortening is an emergent property of the collective motor generated in each half-thick filament by the mechanical coupling between myosin motors via their attachment to the filament backbone. Cell studies have demonstrated that in the intact cell environment, the half-sarcomere is able to efficiently work across a wide range of externally applied loads by tuning the number of heads attached to actin in proportion to the global filament load [4].

Both thin and thick filaments are involved in the regulation of contraction of striated muscle. The classical thin filament mediated mechanism implies that, following the rise of [Ca$^{2+}$] induced by the cell membrane depolarization, Ca$^{2+}$-binding to troponin in the thin filament induces a structural change in the regulatory complex (troponin and tropomyosin) (Fig. 1b) that makes the actin sites available for binding of the myosin motors [5]. On the other end myosin motors in the resting muscle lie on the surface of the thick filament in the OFF state that prevents ATP hydrolysis and attachment to actin [6,7]. A stress-sensing mechanism in the thick filament that switches motors ON to make them available for actin interaction has been recently characterized by combined mechanical and X-ray diffraction studies on intact muscle cells [8,9], but the molecular details of the mechanism and its control by accessory and cytoskeleton proteins (MyBP-C and titin, Fig. 1b) are still poorly understood.

Cell studies, on the other hand, are complicated by the large ensemble of motor proteins and filaments and by the confounding contribution of the sarcomeric (regulatory, accessory and cytoskeleton) proteins. Single-molecule mechanics use purified proteins and thus allow the definition of the pure motor protein action and the comparison between different isoforms or native and mutant or genetically modified proteins. Single-

molecule mechanics, however, suffer from the intrinsic limit in that they cannot investigate the properties that uniquely emerge from the collective motor within the architecture of the half-sarcomere.

These limits are overcome with the realization of a one-dimensional nanomachine titrated to contain the minimum number of motor molecules, which, upon interaction with an actin filament, are able to mimic the half-sarcomere performance generating steady force and constant-velocity shortening [10]. In the nanomachine, an ensemble of myosin II molecules, purified from the skeletal muscle, are carried on a piezo-nanomanipulator and brought to interact with an actin filament attached with the proper polarity to the bead (Bead Tailed Actin, BTA [11]) trapped on the focus of a dual laser optical tweezers (DLOT, [12]). In perspective, the nanomachine has the possibility to selectively test the role of the other sarcomeric proteins by integrating them in the system one at a time. A main limit to this end is that to obtain correctly oriented BTA via gelsolin, a $Ca^{2+}$-regulated actin-binding protein, it is necessary a $[Ca^{2+}]$ of 0.1 mM (corresponding to [free $Ca^{2+}$] of 0.077 mM in the given experimental conditions [13]) [11]. Setting an alternative method that preserves $[Ca^{2+}]$ as a free parameter is compelling for future investigations of the role of any other sarcomeric protein acting through $Ca^{2+}$-dependent mechanisms. Among them, the most important is the $Ca^{2+}$-dependent thin filament activation by the regulatory complex troponin-tropomyosin. The problem is overcome here by exploiting the recent availability of a $Ca^{2+}$-insensitive gelsolin fragment (TL40 from Hypermol, Germany, see Materials and Methods).

The force developed in isometric conditions and the force-velocity (*F-V*) relation of the nanomachine powered by eight HMM fragments of myosin from rabbit psoas in 2 mM ATP are determined either in the absence or in the presence of 0.1 mM $Ca^{2+}$ (the concentration required for BTA preparation with gelsolin). At the same temperature (~23 °C) all the relevant mechanical parameters (the development of the maximum force in isometric conditions ($F_0$), the maximum shortening velocity (the unloaded shortening velocity $V_0$) and the maximum power ($P_{max}$)) are the same independent of the $[Ca^{2+}]$ and the protocol used for BTA assembling. Moreover, once the methodological limits of the *in vitro* mechanics are taken into account, a kinetic model simulation based on the performance of fast mammalian skeletal muscle is able to fit all the relevant mechanical parameters of the nanomachine simply scaling down the number of motors available for actin interaction. The nanomachine with BTA assembled using the $Ca^{2+}$-insensitive gelsolin fragment TL40 preserves $[Ca^{2+}]$ as a free parameter, together with the development of a multiscale model for interfacing data at different hierarchical levels of the striated muscle, open new avenues for investigation of the $Ca^{2+}$-dependent function/dysfunction of any specific sarcomere protein.
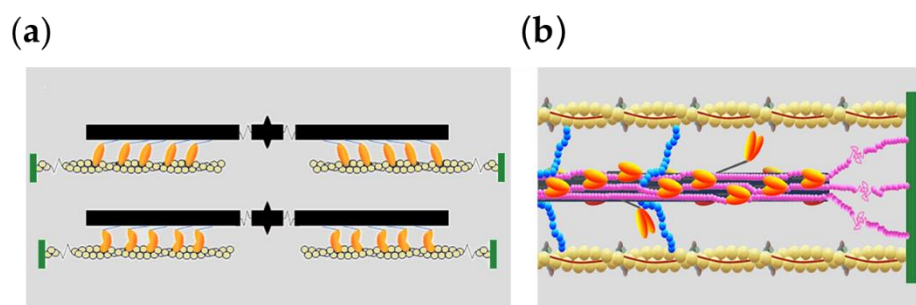


**Figure 1.** (**a**) Cartoon illustrating the sarcomere shortening due to the reciprocal sliding between the myosin filament (black) originating at the centre of the sarcomere (M line) and the actin filament (yellow) originating from the Z line at the end of the sarcomere (green), powered by the interdomain structural change in the S1 fragment of the myosin motor (orange) from the pre- (upper panel) to the post-working stroke conformation (lower panel) . (**b**) Schematic representation of the half-sarcomere protein assembly. Shown are actin (yellow), tropomyosin (Tm, red) and troponin complex (Tn, light and dark gray and brown) on the thin filament. On the thick filament (black) most of the S1 fragments of myosin dimers (orange) lie tilted back (OFF state) and the S1 fragments of two dimers move away with tilting of their S2 rod-like domain (ON state); the MyBP-C (blue) lies on the thick filament with the C-terminus and extends to thin filament with the N-terminus. Titin (pink) in the I-band connects the Z line to the tip of the thick filament and in the A-band runs on the surface of the thick filament up to the M-line at the centre of the sarcomere.

## 2. Results

*2.1. A version of the nanomachine that is independent of the presence/absence of Ca$^{2+}$*

The mechanical output of the synthetic nanomachine powered by myosin II from rabbit psoas in solution with 2 mM ATP was measured either in the presence of Ca$^{2+}$ (0.1 mM CaCl$_2$, BTA prepared with gelsolin) or in Ca$^{2+}$-free solution (BTA prepared with the gelsolin fragment TL40), as described in Methods (see also [10]) (Fig. 2). The ensemble of HMM fragments of myosin, carried on a piezo-nanomanipulator acting as length transducer, is brought to interact with an actin filament attached with the proper polarity to the bead trapped on the focus of a dual laser optical tweezers (DLOT) acting as force transducer (Fig. 2a).

The experiment in Fig. 2b, done in Ca$^{2+}$-free solution with the actin filament attached to the bead via the gelsolin fragment TL40, shows that in position clamp (time interval, $i_t$ 1), following the formation of the actin-myosin interface, the force rises to a maximum steady value ($F_0$) of ~ 16 pN. At this point the control is switched to force ($i_t$ 2) and then a staircase of force drops to 11 ($i_t$ 3), 7 ($i_t$ 4) and 3 pN ($i_t$ 5) is imposed, which elicits shortenings at constant velocity progressively larger as force decreases. When the control is switched back to position clamp ($i_t$ 6), the force recovers a maximum steady value identical to the initial $F_0$, demonstrating that the number of motors available for attachment to the actin filament remains the same throughout the whole interaction.

As shown in Fig. 2c, independent of the presence (dark grey) or the absence of Ca$^{2+}$ (light grey-dashed bars), the frequency distributions of $F_0$ almost superimpose and the mean values are $15.41 \pm 0.73$ pN in 0.1 mM CaCl$_2$ and $15.88 \pm 0.66$ pN in Ca$^{2+}$-free solution. The difference is not significant according to the $t$ test ($P > 0.1$). Thus, there is no significant effect of Ca$^{2+}$ on the isometric force.

The *F-V* relation in either condition is plotted in Fig. 2D (dark grey symbols in 0.1 CaCl$_2$, light grey symbols in Ca$^{2+}$-free solution), showing that the *F-V* points lie along the same relation irrespective of the presence/absence of Ca$^{2+}$. The dashed lines are the fits to the respective *F-V* data using Hill's hyperbolic equation [14]

$$(F+a)\times(V+b) = (F_0+a)\times b \tag{1}$$

In 0.1 mM CaCl$_2$ experiments (dark grey dashed line) $V_0$ (= $b \times F_0/a$, the ordinate axis intercept that estimates the maximum shortening velocity or the velocity of unloaded shortening) and $a/F_0$ (the distance from the vertical asymptote to the ordinate axis, which gives an estimate of the curvature of the *F-V* relation) are $3.41 \pm 0.33$ µm s$^{-1}$ and $0.25 \pm 0.08$ respectively, practically the same as $V_0$ and $a/F_0$ in Ca$^{2+}$-free experiments (light grey dashed line), $3.56 \pm 0.42$ µm s$^{-1}$ and $0.24 \pm 0.09$ respectively. In either case the $t$ test for the differences gives a $P > 0.1$. $V_0$ is ~35% higher than the corresponding $V_f$ (filled symbols, $2.56 \pm 0.43$ µm s$^{-1}$ in Ca$^{2+}$-free conditions and $2.43 \pm 0.41$ µm s$^{-1}$ in solution with 0.1 mM CaCl$_2$), the velocity of filament sliding on rabbit HMM in the *in vitro* motility assay (IVMA). According to the $t$ test the difference is significant with $0.1 > P > 0.05$. A larger difference was previously observed between $V_f$ determined in IVMA with myosin extracted from frog muscle and $V_0$ determined *in situ* in single fibres from the same frog muscle [15] and was attributed to the presence, in the IVMA, of non-specific interactions between actin filaments and the IVMA surface. Putatively, these interactions are less effective in the nanomachine than in the IVMA, suggesting that motors interacting with the actin filament are better exposed to interaction because they lie on a convex surface (Fig. 2a and see Methods).

The power-force (*P-F*) relations calculated from the *F-V* hyperbolic fits are plotted in Fig. 2e and show a $P_{max}$ value of 5.35 aW and 5.51 aW, in 0.1 mM CaCl$_2$ and Ca$^{2+}$-free solution respectively. Thus, as expected from the curvature (defined by the parameter $a/F_0$) also $P_{max}$ is not affected by Ca$^{2+}$. These results demonstrate that the performances of the nanomachine are identical assembling the BTA with either gelsolin (that implies a [Ca$^{2+}$] of 0.1 mM) or the gelsolin fragment TL40 in Ca$^{2+}$-free solution. The use of the TL40 fragment totally preserves the nanomachine performance while makes [Ca$^{2+}$] a free parameter, opening the possibility for studies of the Ca$^{2+}$-dependent mechanisms of the other sarcomere proteins.
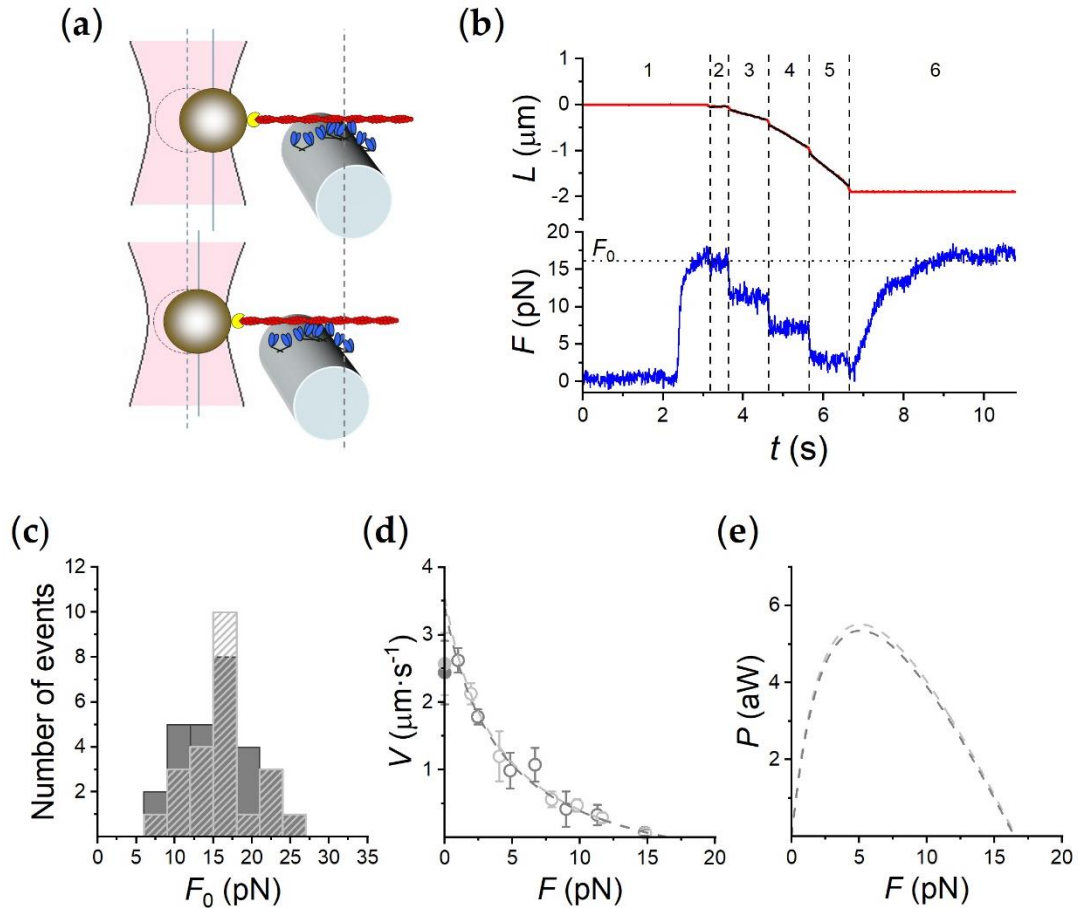
**Figure 2. Performance of the rabbit HMM-based nanomachine.** (**a**) Schematic representation of two snapshots during the interaction between the actin filament and the motor ensemble. Upper panel: in position clamp at $F_0$; lower panel: in force clamp at 0.4 $F_0$. (**b**) Recording of the actin filament sliding ($L$, upper trace, red) and force ($F$, lower trace, blue) during an interaction. Numbers bounded by dashed lines identify the different time intervals ($i_t$) as detailed in the text. (**c**) Frequency distribution of $F_0$. Data are plotted in classes of 3 pN; dark grey bars, measurements in 0.1 mM $CaCl_2$ (= 77 µM free $[Ca^{2+}]$); light grey-dashed bars, in the absence of $Ca^{2+}$. (**d**) $F$-$V$ relation. Data are from 28 experiments in 0.1 mM $CaCl_2$ (dark grey open circles) and 23 experiments in $Ca^{2+}$-free solution (light grey open circles). Points are mean ± SD from individual experiments, grouped in classes of force $0.15F_0$ wide. Dark and light grey filled symbols on the ordinate are the $V_f$ in the IVMA on rabbit HMM with and without $Ca^{2+}$ respectively. The dashed lines are Hill's hyperbolic equation fits to the data with the same color code as symbols. (**e**) Power ($P$) versus $F$, calculated from the corresponding $F$-$V$ fits in d, with the same color code.

## 2.2. Interfacing in vitro and in situ performance of myosin II by model simulation

The power of the nanomachine to define the emergent properties of the half-sarcomere of striated muscle is tested by applying the same mechano-kinetic model of the actin-myosin interaction to fit the performances of both the nanomachine powered by myosin II from rabbit psoas muscle and the intact fast mammalian muscle. As shown in Fig. 3a (from [10]), the model is based on one detached state (D) and two different force-generating attached states (A1 and A2). The kinetics of state transitions is firstly constrained to fit the mechanics and energetics of the skeletal muscle. In the absence of a direct estimate of the mechanical parameters of the intact fast rabbit muscle, the muscle of reference that provides adequate mechanical and energetic information to be used as constraints for interfacing with *in vitro* results is the extensor digitorum longus (EDL) from the rat ([16] and references therein). This may imply a 10% overestimation of the kinetic parameters used in the simulation of rabbit muscle, due the smaller size of the rat, on the basis the size effect

on ortholog myosin isoforms [17]; however, for reason of simplicity we did not apply any correction in adapting the rat muscle parameters for the rabbit myosin nanomachine.

The mechanical constraints from the whole muscle experiments at the temperature of the nanomachine experiments (24°C) are: (*i*) isometric tetanic force $F_0$ 250 kPa, (*ii*) unloaded shortening velocity $V_0$ 8.6 μm s$^{-1}$ per half-sarcomere, (*iii*) *F-V* relation as in Fig. 3b, in which the data from [16] and references therein are fitted with Hill hyperbolic equation (dashed line), which gives a value of $a/F_0$ (the parameter that estimates the curvature of the relation) of 0.36. The density of force per cross-sectional area can be translated to force per half thick filament (htf) taking into account the thick filament density ($\sim$5.8.10$^{14}$ m$^{-2}$, [18] and references therein) and corresponds to 460 pN per htf (see abscissa intercept of the dashed line in Fig. 3b). The power-force (*P-F*) relation, calculated from the *F-V* relation, shows a maximum power ($P_{max}$) of 460 aW per htf attained at $\sim$1/3 $F_0$ (Fig. 3c, dashed line).

Model simulations of mechanics and energetics of the muscle (Fig. 3b and c and Table 1) are obtained by adjusting the rate functions governing the kinetics of state transitions as shown in Supplementary Fig. 1. The coupling between mechanical and biochemical steps in the cycle of Fig. 3 has been already described in detail [10] and is synthetically reported in Methods. The most relevant energetic features, and how they are constrained by data in the literature is explained here following. In isometric contraction the rate-limiting step in the cycle is detachment from A2: under these conditions the fraction of motors attached (the duty ratio) is maximum, while the rate of ATP splitting per myosin head ($\varphi_0$) is minimum (at room temperature it is $\sim$11 s$^{-1}$ for the mammalian muscle ([19] and references therein). During steady shortening the duty ratio decreases and the ATP splitting rate per myosin head ($\varphi$) increases, due to the increase in the rate of motor detachment following the working stroke [20-23]. However, $\varphi$ at the load for the maximum power ($\varphi_{Pmax}$) is higher than $\varphi_0$ by no more than 3 times [19], so that the resulting maximum power can be predicted only by assuming that, during shortening, the attached myosin motors can rapidly regenerate the working stroke by slipping to the next actin farther from the centre of the sarcomere during the same ATPase cycle [21,23,24] (step "slip" in Fig. 3a) and undergoing A1'- A2' state equilibration according to step 2 kinetics [1]. Detachment from either A1' or A2' (step 3') implies ATP hydrolysis. As shown in Fig. 3b and c and in Table 1, the relations and the underlying mechanical and energetic parameters predicted by the model for the half-sarcomere of the mammalian muscle agree with those derived from published data [16,19]. Notably, $\varphi_0$ calculated by the flux through step 1 at $F_0$, is 11.6 s$^{-1}$. At $P_{max}$, $\varphi_{Pmax}$ increases to 35.5 s$^{-1}$ in the mammalian muscle ($\sim$3·$\varphi_0$).

The nanomachine performances, represented by open circles and dashed lines in Fig. 3d and by the dashed line in e, where the *F-V* and *P-F* relations are obtained by pooling data in the absence and the presence of Ca$^{2+}$ from Fig. 2, are simulated after taking into account the effects of the methodological limits of the *in vitro* system with respect to muscle: (*i*) the compliance in series with the system constituted by the motor array and the overlapping bead-attached actin filament must be raised by two orders of magnitude with respect to that of a muscle cell [10] to include the trap compliance, 3.7 nm pN$^{-1}$; (*ii*) evidence from single molecule mechanics indicate that the random orientation of the motors on their support reduces the force developed at high load from the value exerted by the correctly oriented motor ($F_c$) down to a minimum value of 0.1$F_c$ attained when the motors are 180° away from the correct orientation [25]; (*iii*) similarly single molecule mechanics showed that the step size (*L*) generated at low load by a motor lying on a cofilament (in which a few myosin molecules lie on a LMM backbone) is reduced with respect to that ($L_c$ $\sim$10 nm) of the motor interacting with a correctly oriented actin filament, when the actin filament is oriented in the opposite direction [26]. These constraints are introduced in the model by reducing progressively with the deviation from the correct orientation (0°) the isometric force and the shortening range for which an attached force generating motor (A2 state) maintains force, according to the family of A2 force functions shown in Supplementary Fig. 2a (light red lines). The relevant parameters describing the force function range from $F_c$ = 5 pN and $L_c$ = 10 nm, exhibited by a correctly oriented motor (black line from Supplementary Fig. 6b in [10]), to 0.5 pN and 1.5 nm respectively (red line) exhibited by a motor 180° away from the correct orientation. Correspondingly the slope of the A1 force function, representing the stiffness of the attached motor, scales from 2 pN nm$^{-1}$ (black dashed line) to 0.2 pN nm$^{-1}$ (red dashed line). This is a quite sensible assumption considering that for a motor away from the correct orientation also the S2 domain can contribute to the compliance [27,28].

Under these conditions the model is able to fit all the features of the *F-V* and *P-F* relations of the myosin-based nanomachine (continuous lines in Fig. 3d and e respectively), using as only free parameter the number of motors available for the actin interaction (*N*), which must be scaled down from that in the half-thick filament, 294 [29], to that in the nanomachine, 16 in those experiments [10]. This is shown in detail in Fig. 3f, in which

the horizontal dashed lines, representing the experimental values for $F_0$ (16.79 ± 0.38 pN), $P_{max}$ (5.45 aW) and $V_0$ (3.54 ± 0.13 μm s$^{-1}$), intersect the relations between the corresponding simulated parameters and $N$ (dots) for $N = 16$. 16 is twice the number of rupture events recorded from the ensemble of motors deposited on the same support in ATP-free (rigor) conditions (see Fig. 1 in [10]). Assuming that each motor of the myosin dimers identified as available for actin interaction by rupture events in rigor behaves independently in 2 mM ATP, eight rupture events in rigor imply $N = 16$ in agreement with the prediction of the model simulation.

The application of the model simulation to the nanomachine implies, beyond the depressant effect of the random orientation of motors on both the step size and force of the motor (Supplementary Fig. 2a) the introduction of a one hundred times larger series compliance, which causes the strain-dependent kinetics of the attached motors to generate the push-pull experienced by the motors when actin slides away from-toward the bead for the addition-subtraction of the force contribution by each motor, as described in detail in [10]. As a consequence, the model predicts that, with respect to the values in the corresponding muscle, $\varphi_0$ increases by 70% (Table 1). At $P_{max}$ the model predicts that the nanomachine undergoes an increase in $\varphi_{Pmax}$ smaller than that of the muscle (Table 1) as a consequence of the depression in the step size and thus in the low-load velocity of shortening, due to the random orientation of motors.
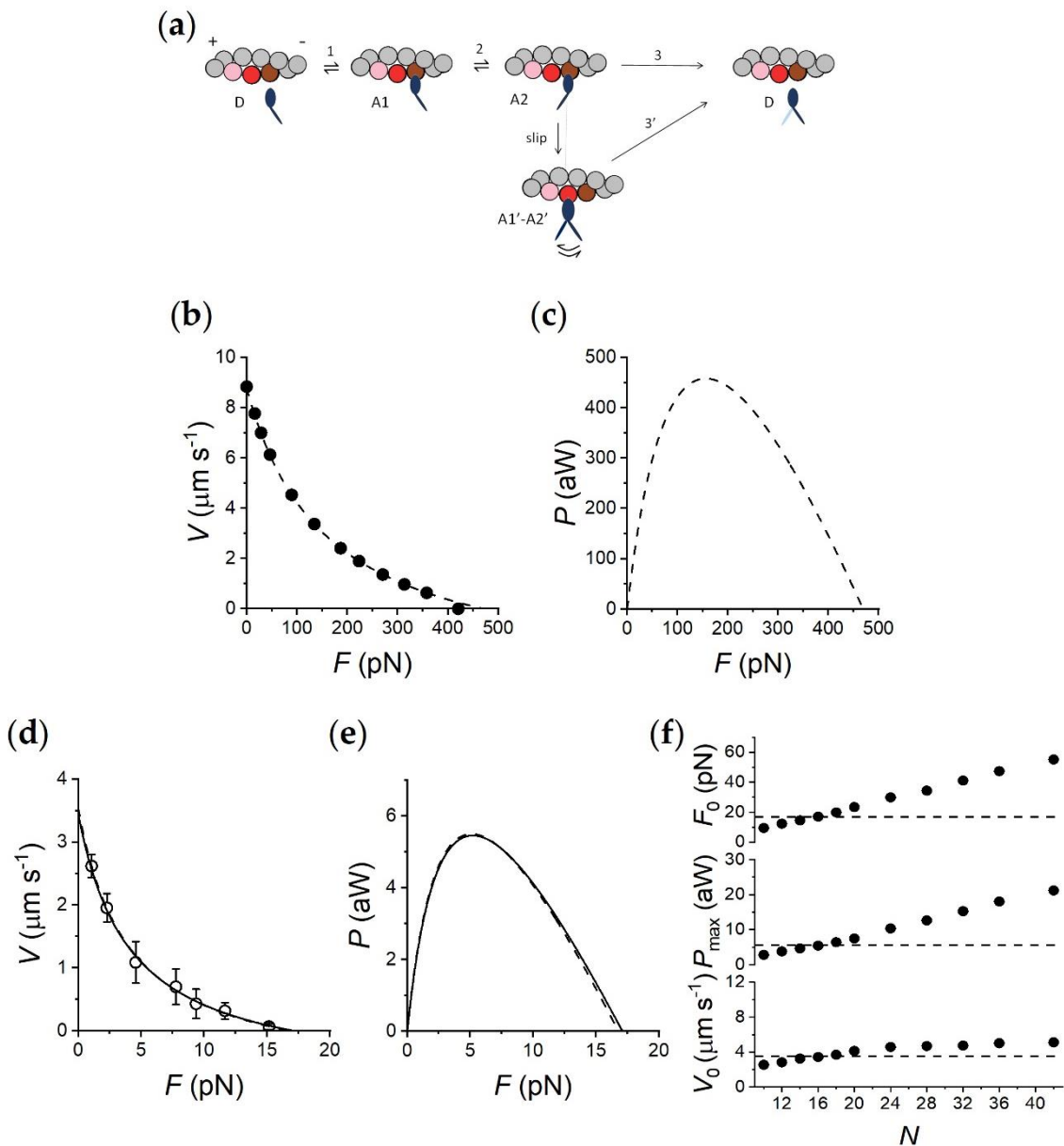


**Figure 3. Model simulation.** (a) Kinetic scheme from Fig. 4A of [10], with three states of the myosin motor (blue): D, detached; A1 and A2, attached to an actin monomer (brown). During shortening the motor attached

in the A2 state can slip to the next actin monomer farther from the centre of the sarcomere (red) within the same ATPase cycle. The probability of a second slipping to the pink monomer is limited to 1/10 of that of the first slipping. (**b**) Simulation of the *F-V* relation of fast mammalian muscle (adapted from Supplementary Fig. 6F in [10]). The experimental *F-V* relation (filled circles) is calculated for the half-sarcomere at full overlap (294 motors available) from the data of fast mammalian muscle at room temperature [30,31]. The dashed line is Hill's hyperbolic equation fitted to the results of the model simulation with a series compliance similar to that in situ (0.01 nm pN$^{-1}$). (**c**) *P-F* relation calculated from Hill's fit in b. (**d**) Experimental *F-V* relation obtained by pooling data in the absence and the presence of Ca$^{2+}$ from Fig. 2 (open circles) and fitted by Hill's hyperbolic equation (dashed line), and its simulation calculated for a number of available heads *N* = 16 (continuous line). (**e**) Corresponding *P-F* relations. (**f**) Dependence on *N* of the three parameters featuring the machine performance, as indicated in the ordinate of each plot. The dashed lines indicate the respective experimental values.

**Table 1. Simulated mechanical and energetic parameters of the muscle half-sarcomere and of the nanomachine.** The parameters reported in the Table are defined below and are accompanied by the references that provide the standard values used to constrain the simulation at the level of the muscle half-sarcomere. *N,* number of available motors, which, per half-thick filament, are (49 crowns x 6 motors per crown =) 294 [29]; $F_0$, isometric force referred to the half-thick filament [16]; $r_0$, isometric duty ratio [32]; $\varphi_0$, flux through step 1 of the cycle in Fig. 3a in isometric condition, corresponding to the ATP hydrolysis rate per myosin head at $F_0$ [19] and references therein; $V_0$, maximum shortening velocity [16]; $P_{max}$, maximum power; $\varphi_{Pmax}$, ATP hydrolysis rate per myosin head at $P_{max}$ [19,33].

| | $F_0$ (pN) | $r_0$ | $\varphi_0$ (s$^{-1}$) | $V_0$ (µm s$^{-1}$) | $P_{max}$ (aW) | $\varphi_{Pmax}$ (s$^{-1}$) |
|---|---|---|---|---|---|---|
| *N* = 294 Compliance 0.01 nm pN$^{-1}$ | 433 ± 5 | 0.32 | 11.65 | 8.61 ± 0.16 | 462 | 35.50 |
| *N* = 16 Compliance 3.7 nm pN$^{-1}$ + random | 15.8 ± 0.4 | 0.40 | 18.21 | 3.45 ± 0.13 | 5.45 | 26.21 |

## 3. Discussion

A synthetic nanomachine, made by an array of eight myosin dimers of myosin II from the fast skeletal muscle of rabbit interacting with an actin filament, is used to mimic the emergent properties of the half-sarcomere of striated muscle, namely generation of steady force and constant velocity shortening, in the absence of the effects of the other sarcomere (regulatory, accessory and cytoskeleton) proteins. The role of the other sarcomeric proteins can be tested by integrating them in the system one at a time, but in the original system [10] this perspective had a main limit in the use of gelsolin, a Ca$^{2+}$-regulated actin-binding protein, to attach the actin filament with the correct polarity to the bead (BTA) trapped in the focus of the DLOT used as force transducer. In fact, future investigation of the role of any other sarcomeric protein acting through Ca$^{2+}$-dependent mechanisms requires to preserve [Ca$^{2+}$] as a free parameter. The problem is solved here by devising a new protocol in which the BTA is prepared using the Ca$^{2+}$-insensitive gelsolin fragment TL40. The effect of Ca$^{2+}$ on the performance of the nanomachine in its simplest version (eight HMM fragments from the fast isoform of rabbit myosin II pulling on an actin filament) is tested, demonstrating that none of the relevant mechanical parameters, the isometric force $F_0$ (16.8 pN), the unloaded shortening velocity $V_0$ (3.5 µm s$^{-1}$) and the maximum power $P_{max}$ (5.5 aW), depends on the presence/absence of Ca$^{2+}$. Thus, the use of the TL40 fragment to prepare the BTA totally preserves the nanomachine performance while makes [Ca$^{2+}$] a free parameter, opening the possibility for studies of the Ca$^{2+}$-dependent mechanisms of the other sarcomere proteins.

A simplified mechano-kinetic scheme (Fig. 3a) is used first to fit the functional features of the fast mammalian skeletal muscle and then scaled down to the dimension of the synthetic machine powered by eight HMM fragments from the rabbit psoas myosin. The bulk of mechanical and energetic data present in the literature of mammalian muscle [16,19] are taken into account to constrain the rate functions of state transitions (Supplementary Fig. 1) at the temperature (24 °C) of the nanomachine experiments.

The present version of the model is an implementation of that already published [10] in which the predicted $F$-$V$ relation (dotted line in Supplementary Fig. 2b from Fig. 4 of [10]), provided higher than observed shortening velocities in the region of very low loads. The reason of the discrepancy is the absence of consideration, in the previous model simulation, of the depressant effect on the step size of moving away from the correct motor orientation with respect to the actin filament [26]. In Supplementary Fig. 2a the family of light red continuous lines show the effect on the $d$-dependence of the force of A2 motors of the progressive deviation of motor orientation from the correct orientation (green continuous line) to the orientation in the opposite direction (red continuous line). It must be noted that the observed $F$-$V$ relation (circles and dashed line in Fig. 3d and Supplementary Fig. 2b) is predicted by the model (continuous line) only if the values of both $d$ for which the A2 motors maintain the isometric force and the abscissa intercept the A2 force function are scaled down in proportion to the reduction of the isometric force (the ordinate intercept in Supplementary Fig. 2a). Single molecule experiments reporting a smaller effect of opposite orientation on the low load step size than on the force [26] would suggest a reduced effect of wrong motor orientation on the abscissa intercept of the A2 force function. However, reducing any depressant effect on the abscissa intercept of the A2 force function lower than that to that shown by the family of curves in Supplementary Fig 2a makes the simulated low load region of the $F$-$V$ relation to shift above the observed one.

The evidence that a property of the motor array like $V_0$ can be predicted by adjusting a single molecule parameter like the step size is a remarkable demonstration of the efficiency of our approach as a tool for interfacing single motor properties with the properties emerging from its collective arrangement. Moreover, the implementation of a unique model able to fit *in vitro* data from the nanomachine and *in situ* data from the intact muscles accounting for the methodological reasons that limit the nanomachine performance when it fails to get the expected muscle performance generates an unprecedented two-way communicating path. From one side the model allows the definition of the minimal conditions of the synthetic nanomachine able to reproduce the power and efficiency shown at muscle level, from the other the model and the nanomachine integrate to provide a new powerful tool for future applications in which the performance of the synthetic machine powered by mutant and engineered myosins can be exploited to predict their outcome at the organ level.


## 4. Materials and Methods

### 4.1. Preparation of proteins

Adult male rabbits (New Zealand white strain), provided by Envigo, were housed at Centro di servizi per la Stabulazione Animali da Laboratorio (CeSAL) University of Florence, under controlled conditions of temperature ($20 \pm 1°C$) and humidity ($55 \pm 10\%$), and were euthanized by injection of an overdose of sodium pentobarbitone ($150$ mg kg$^{-1}$) in the marginal ear vein, in accordance with the Italian regulation on animal experimentation (Authorization 956/2015-PR) in compliance with Decreto Legislativo 26/2014 and EU directive 2010/63. Two rabbits were used for the experiments.

HMM fragment of myosin was prepared from rabbit psoas muscle as reported previously [10]. The functionality of the purified motors was always preliminarily checked with in vitro motility assay.

Actin was prepared from leg muscles of the rabbits according to [34]. Polymerized F-actin was fluorescently labelled by incubating it overnight at 4°C with excess of phalloidin-tetramethyl rhodamine isothiocyanate [35].

The correct polarity of the actin filament, that is its attachment to the bead with the barbed (+) end [10], was obtained in two ways: (*i*) in the conventional way [11], the +end of the filament was attached to a polystyrene bead (diameter 3 µm) with the Ca$^{2+}$-sensitive capping protein gelsolin, (*ii*) according to a new protocol, in which full-length gelsolin (subdomains S1-S6) was replaced by the Ca$^{2+}$-insensitive gelsolin fragment TL40, consisting of the N-terminal homologous subdomains S1-S3 (Hypermol, Germany), so that the nanomachine could be assembled in the absence of Ca$^{2+}$. In preliminary tests Ca$^{2+}$ was removed from the solutions at various stages of TL40-coated bead preparation, showing no differences in the ability and the specificity to bind the actin filament. Gelsolin-coated beads and TL40-coated beads were stored in the stock

solution (150 mM NaCl, 20 mM sodium phosphate buffer pH 7.4, 0.1 mM ATP, 10 mg ml$^{-1}$ BSA, 5% (v/v) glycerol, and 3 mM NaN$_3$) at 0 °C for about 6 months.

### 4.2. Mechanical measurements

The mechanical apparatus is described in detail in [10]. Briefly, the myosin motors, deposited on the functionalized surface of a chemically etched single-mode optical fiber carried on a 3-way piezoelectric nanopositioner (nano-PDQ375, Mad City Lab, Madison WI, USA) acting as a displacement transducer, are brought to interact with an actin filament attached with the correct orientation to the bead (bead tailed actin, BTA) trapped in the focus of a Dual Laser Optical Tweezers (DLOT, [12]) acting as a force transducer. The force-displacement transducer system has a dynamic range for both force (0-200 pN, resolution 0.3 pN) and displacement (0-75000 nm, resolution 1.6 pN) adequate to measure the output of the nanomachine and can be servo-controlled either in position or force feedback [10,36]. The frequency response of the system in position feedback is limited by the rise time of the piezo-stage movement ($t_r$ ~2 ms), while in force feedback it is limited also by the damping exerted on the bead by the viscosity of the medium so that $t_r$ is ~20 ms. Mechanical protocols are described in the section Results. For all the experiments [HMM] was 100 µg ml$^{-1}$ [10].

The nanomachine is hosted in a flow chamber which has two separate compartments in which actin and myosin were flowed separately, thereby preventing uncontrolled protein interactions: one compartment was used to introduce the bead-attached actin, the other compartment, in which the support for the myosin motors was mounted, to introduce HMM dissolved in buffer A (25 mM imidazole pH 7.4, 33 mM KCl, 0.1 mM CaCl$_2$, 5 mM MgCl$_2$, 10 mM DTT and 2 mM ATP) [10]. The support for the motors was the lateral surface of a single-mode optical fiber, chemically etched to a diameter of ~4 µm and functionalised for HMM attachment by coating with nitrocellulose (1% w/v) [35]. The fiber was positioned in the HMM compartment just before the confluence of the two compartments. Actin-attached beads from the other compartment were trapped with the optical tweezers one by one at the intersection of the flows to select that with a single actin filament at least 6–7 µm long. Then the flow chamber was moved across the x-y planes by means of a micro-positioner carrying the nanopositioner to bring the bead-attached actin close to the support with the motor array. The final positioning was achieved under nanopositioner control. To start the experiment, buffer B (buffer A plus 0.1 mg ml$^{-1}$ glucose oxidase, 20 µg ml$^{-1}$ catalase, 5 mg ml$^{-1}$ glucose plus 0.5% w/v methylcellulose, 400 cP) was flowed at 10 µl min$^{-1}$. The presence of methylcellulose inhibited the lateral diffusion of F-actin [37], thereby minimising the probability that, in 2 mM ATP, the interaction terminates during low-force isotonic contractions or during the initial phases of force redevelopment following large releases. 0.5% w/v methylcellulose did not affect the mechanical and kinetic properties of the nanomachine [10]. All experiments were conducted at 23°C.

### 4.3. Data analysis

The velocity of shortening ($V$, µm s$^{-1}$) in the responses to reduction of force to $F$ values (pN) below the isometric value ($F_0$) was measured by the slope of the displacement trace (the red trace interpolated with black lines for clarity in Fig. 2B). The $F$-$V$ data were fitted with the hyperbolic Hill equation [14]: $(F + a)(V + b) = (V_0 + b)a,$ where $a$ and $b$ are the distances of the asymptotes from the ordinate and abscissa, respectively, and $V_0$ (the ordinate intercept) estimates the maximum or unloaded shortening velocity. $a$ is a parameter that is used to express the degree of curvature of the relation. $a$ has the dimension of a force (pN) and, when normalised for $F_0$, is an index of the relative maximum power that can be delivered at intermediate forces [14]. The power output ($P$) at any force was calculated by the product between $F$ and $V$ and expressed as µm s$^{-1}$ · pN = 10$^{-18}$ W = aW. Dedicated programs written in LabVIEW (National Instruments) and Origin 2015 (OriginLab Corporation) were used for the analysis. Experimental points are expressed as mean ± SEM unless otherwise stated.

### 4.4. Mechano-kinetic model

The results were numerically simulated by a stochastic model already published [10] that estimates the probability distributions of potential results by allowing for random variation in inputs over time until the Standard Deviation of the result is lower than 5%. The mechanical cycle of the motors is depicted in Fig. 3a.

The state transitions as well as the strain of the attached motors are stochastically determined according to the kinetics reported in supplementary Fig. 1. Each attached motor exerts, on the actin filament, a force that depends on its conformation and its position with respect to the actin monomer to which it is attached. The model operates either in position or force clamp. The iteration time in the calculation of the dependent variable, $\Delta t$ ($= 10^{-5}$-$10^{-6}$ s), depends on the stiffness of the system, which is dominated by the trap compliance. Both the force generated by the motors, transmitted through the BTA, and the force of the optical trap act on the trapped bead. The motion of the bead was simulated with over-damped dynamics by using a drag coefficient calculated from the bead radius and the viscosity of the medium (Stokes' Law). In this way the bead displacement in response to a stepwise change in force showed a rise time $t_r$ similar to that measured experimentally (20 ms).

The kinetic scheme used to simulate the output of the nanomachine is based on three states of the myosin motors (one detached, D, and two force-generating attached states, A1 and A2 (Fig. 3a). The stiffness of the correctly oriented attached motors is 2 pN nm$^{-1}$ [10], taken as an average from [27,32,38], and the kinetics of the state transitions are selected on the basis of the mechanical and energetic properties of the corresponding intact muscles, as detailed in the text. Detached motors (D), with the hydrolysis products (ADP and inorganic phosphate, $P_i$) in the catalytic site, attach to the actin monomer (5 nm in diameter) (D$\rightarrow$A1, step 1) at values of $d$ (the relative axial position between the motor and the actin monomer with $d = 0$ when the force in A1 is zero) ranging from -2.5 to 2.5 nm, according to the principle of the nearest-neighbor interaction. Following the state transition A1$\rightarrow$A2 (step 2), the motors undergo the working stroke that accounts for the generation of force at $d = 0$ and its maintenance during shortening [1,21]. The working stroke, accompanied by Pi release, is a multistep reaction the extent and speed of which depend on the degree of shortening and external load [21,23]. During isotonic shortening, the speed of the working stroke is fast enough for the reaction to be considered at the equilibrium and the A2 force to follow the $d$- dependence shown in Supplementary Fig. 2a, black continuous line [1,21]. In the nanomachine, the depressant effect of the random orientation of motors on the force and the step size is taken into account reducing the force and sliding distance for which the A2 motor maintains force from the values exhibited by the correctly oriented motor ($F_c$ = 5 pN and $L_c$ = 10 nm, respectively) in proportion to the deviation from correct orientation (light red lines) up to a minimum of 0.5 pN and 1.5 nm respectively (red line) for the orientation at 180°. The instantaneous stiffness of A1 motors reduced accordingly (dashed lines) and became 0.2 pN nm$^{-1}$ for the orientation at 180°. The A2 motors detach (A2$\rightarrow$D, Fig. 3a step 3) following ADP release and ATP binding with a speed that, under physiological [ATP] ($\geq$ 2 mM), is dictated by the conformation-dependent kinetics of ADP release [4,22,23]. In order to maintain the scheme simple, the hydrolysis step and the repriming of the working stroke are incorporated in state D and contribute to the limited speed of the attachment reaction. The rate functions for the state transitions depend on $d$ as shown in fig. S1. As detailed in the text, the rate functions are first defined to simulate the mechanics and energetics of the intact muscle and then used to fit the output of the nanomachine.

**Conflicts of Interest:** The authors declare no conflict of interest. The funders had no role in the design of the study; in the collection, analyses, or interpretation of data; in the writing of the manuscript, or in the decision to publish the results.

# References

1. Huxley, A.F.; Simmons, R.M. Proposed mechanism of force generation in striated muscle. *Nature* **1971**, *233*, 533-8.
2. Rayment, I; Holden, H.M.; Whittaker, M.; Yohn, C.B.; Lorenz, M.; Holmes, K.C.; Milligan, R.A. Structure of the actin-myosin complex and its implications for muscle contraction. *Science* **1993**, *261*, 58-65.
3. Lymn, R.W.; Taylor, E.W. Mechanism of adenosine triphosphate hydrolysis by actomyosin. *Biochemistry* **1971**, *10*, 4617-24.
4. Piazzesi, G.; Reconditi, M.; Linari, M.; Lucii, L.; Bianco, P.; Brunello, E.; Decostre, V.; Stewart, A.; Gore, D.B.; Irving, T.C.; Irving, M.; Lombardi, V. Skeletal muscle performance determined by modulation of number of myosin motors rather than motor force or stroke size. *Cell* **2007**, *131*, 784-95.
5. Gordon, M.; Homsher, E.; Regnier, M. Regulation of contraction in striated muscle. *Physiol Rev*. **2000**, *80*, 853-924.
6. Woodhead, J.L.; Zhao, F.Q.; Craig, R.; Egelman, E.H.; Alamo, L.; Padrón, R. Atomic model of a myosin filament in the relaxed state. *Nature* **2005**, *436*(7054):1195-9.
7. Stewart, M.A.; Franks-Skiba, K.; Chen, S.; Cooke, R. Myosin ATP turnover rate is a mechanism involved in thermogenesis in resting skeletal muscle fibers. *Proc Natl Acad Sci U S A* **2010**, *107*(1):430-5.
8. Linari, M.; Brunello, E.; Reconditi, M.; Fusi, L.; Caremani, M.; Narayanan, T.; Piazzesi, G.; Lombardi, V.; Irving, M. Force generation by skeletal muscle is controlled by mechanosensing in myosin filaments. *Nature* **2015**, *528*(7581):276-9.
9. Reconditi, M.; Caremani, M.; Pinzauti, F.; Powers, J.D.; Narayanan, T.; Stienen, G.J.; Linari, M.; Lombardi, V.; Piazzesi, G. Myosin filament activation in the heart is tuned to the mechanical task. *Proc Natl Acad Sci U S A* **2017**, *114*(12):3240-3245.
10. Pertici, I.; Bongini, L.; Melli, L.; Bianchi, G.; Salvi, L.; Falorsi, G.; Squarci, C.; Bozó, T.; Cojoc, D.; Kellermayer, M.S.Z.; Lombardi, V.; Bianco, P. A myosin II nanomachine mimicking the striated muscle. *Nat Commun*. **2018**, *9*, 3532.
11. Suzuki, N.; Miyata, H.; Ishiwata, S.; Kinosita, K.Jr. Preparation of bead-tailed actin filaments: estimation of the torque produced by the sliding force in an in vitro motility assay. *Biophys J*. **1996**, *70*, 401-8.
12. Bianco, P.; Bongini, L.; Melli, L.; Dolfi, M.; Lombardi, V. PicoNewton-millisecond force steps reveal the transition kinetics and mechanism of the double-stranded DNA elongation. *Biophys J*. **2011**, *101*, 866-74.
13. Bers, D.M.; Patton, C.W.; Nuccitelli, R. A Practical Guide to the Preparation of Ca2+ Buffers, In *Calcium in Living Cells*, Whitaker, M., Ed; Elsevier, 2010; Volume 99, pp. 1-26.
14. Hill, A. V. The heat of shortening and the dynamic constants of muscle. *Proc. R. Soc. B* **1938**, *126*, 136–195.
15. Elangovan, R.; Capitanio, M.; Melli, L.; Pavone, F.S.; Lombardi, V.; Piazzesi, G. An integrated in vitro and in situ study of kinetics of myosin II from frog skeletal muscle. *J Physiol*. **2012**, *590*, 1227-42.
16. Ranatunga, K.W. Temperature Effects on Force and Actin-Myosin Interaction in Muscle: A Look Back on Some Experimental Findings. *Int J Mol Sci*. **2018**, *19*, 1538.
17. Reggiani, C.; Bottinelli, R.; Stienen, G.J. Sarcomeric Myosin Isoforms: Fine Tuning of a Molecular Motor. *News Physiol Sci*. **2000**, *15*, 26-33.
18. Percario, V.; Boncompagni, S.; Protasi, F.; Pertici, I.; Pinzauti, F.; Caremani, M. Mechanical parameters of the molecular motor myosin II determined in permeabilised fibres from slow and fast skeletal muscles of the rabbit. *J Physiol*. **2018**, *596*, 1243-1257.
19. Barclay, C.J. Energetics of contraction. *Compr Physiol.* **2015,** *5*, 961-95.
20. Huxley, A.F. Muscle structure and theories of contraction. *Prog Biophys Biophys Chem*. **1957**, 7, 255-318.
21. Piazzesi, G.; Lombardi, V. A cross-bridge model that is able to explain mechanical and energetic properties of shortening muscle. *Biophys J*. **1995**, *68*, 1966-79.
22. Nyitrai, M.; Geeves, M.A. Adenosine diphosphate and strain sensitivity in myosin motors. *Philos Trans R Soc Lond B Biol Sci*. **2004**, *359*, 1867-77.

23. Caremani, M.; Melli, L.; Dolfi, M.; Lombardi, V.; Linari, M. The working stroke of the myosin II motor in muscle is not tightly coupled to release of orthophosphate from its active site. *J Physiol*. **2013**, *591*, 5187–5205.

24. Lombardi, V.; Piazzesi, G.; Linari, M. Rapid regeneration of the actin-myosin power stroke in contracting muscle. *Nature* **1992**, *355*, 638-41.

25. Ishijima, A.; Kojima, H.; Higuchi, H.; Harada, Y.; Funatsu, T.; Yanagida, T. Multiple- and single-molecule analysis of the actomyosin motor by nanometer-piconewton manipulation with a microneedle: unitary steps and forces. *Biophys J*. **1996**, *70*, 383-400.

26. Tanaka, H.; Ishijima, A.; Honda, M.; Saito, K.; Yanagida, T. Orientation dependence of displacements by a single one-headed myosin relative to the actin filament. *Biophys J*. **1998**, *75*, 1886-94.

27. Kaya, M. & Higuchi, H. Nonlinear elasticity and an 8-nm working stroke of single myosin molecules in myofilaments. *Science* **2010**, *329*, 686-689.

28. Linari, M.; Piazzesi, G.; Pertici, I.; Dantzig, J.A.; Goldman, Y.E.; Lombardi, V. Straightening Out the Elasticity of Myosin Cross-Bridges. *Biophys J*. **2020**, *118*, 994-1002.

29. Craig, R.; Offer, G. Axial arrangement of crossbridges in thick filaments of vertebrate skeletal muscle. *J Mol Biol*. **1976**, *102*, 325-32.

30. Ranatunga, K.W. Temperature-dependence of shortening velocity and rate of isometric tension development in rat skeletal muscle. *J Physiol.* **1982**, *329*, 465-83.

31. Ranatunga, K.W. The force-velocity relation of rat fast- and slow-twitch muscles examined at different temperatures. *J Physiol.* **1984**, *351*, 517-29.

32. Linari, M.; Caremani, M.; Piperio, C.; Brandt, P.; Lombardi, V. Stiffness and fraction of Myosin motors responsible for active force in permeabilized muscle fibers from rabbit psoas. *Biophys J*. **2007**, *92*, 2476-90.

33. Barclay, C.J.; Woledge, R.C.; Curtin, N.A. Inferring crossbridge properties from skeletal muscle energetics. *Prog Biophys Mol Biol*. **2010**, *102*, 53-71.

34. Pardee, J.D.; Spudich, J.A. Purification of muscle actin. *Methods Enzymol*. **1982**, *85*, 164-81.

35. Kron, S.J.; Toyoshima, Y.Y.; Uyeda, T.Q.; Spudich, J.A. Assays for actin sliding movement over myosin-coated surfaces. *Methods Enzymol*. **1991**, *196*, 399-416.

36. Bianco, P.; Bongini, L.; Melli, L.; Falorsi, G.; Salvi, L.; Cojoc, D.; Lombardi, V. Fast Force Clamp in Optical Tweezers: A Tool to Study the Kinetics of Molecular Reactions, In *Novel Approaches for Single Molecule Activation and Detection*; Benfenati, F., Di Fabrizio, E., Torre, V., Eds; Springer Berlin, Heidelberg, 2014; pp. 123–147.

37. Uyeda, T.Q.; Kron, S.J.; Spudich, J.A. Myosin step size. Estimation from slow sliding movement of actin over low densities of heavy meromyosin. *J. Mol. Biol*. **1990**, *214*, 699-710.

38. Lewalle, A.; Steffen, W.; Stevenson, O.; Ouyang, Z.; Sleep, J. Single-molecule measurement of the stiffness of the rigor myosin head. Biophys J. **2008**, *94*, 2160-9.